Robust Tracking of Longitudinal Objects Lying on the Sea Floor with an AUV equipped of a Scanning Sonar

Christian Barat
Laboratoire I3S (Informatique, Signaux et Systèmes de Sophia Antipolis)
2000 route des Lucioles, BP 121, 06903 Sophia Antipolis cedex, FRANCE
barat@i3s.unice.fr

Maria João Rendas
Laboratoire I3S (Informatique, Signaux et Systèmes de Sophia Antipolis)
2000 route des Lucioles, BP 121, 06903 Sophia Antipolis cedex, FRANCE
rendas@i3s.unice.fr

***Abstract* - The paper considers the problem of using an autonomous underwater platform equipped of a scanning profiler sonar to track elongated objects lying on the sea floor, e.g. pipelines. The algorithm presented assumes the existence of features that enable the discrimination between sonar profiles received from the tracked object and those received from the background sea bottom. The algorithm does not require explicit classification of the profiles received (as coming from the tracked object or from the sea bottom), and does not rely on reconstruction of the geometry of the surface of the tracked object (alowing tracking of proud or partially buried objects). Simulation results illustrate the performance of the algorithm presented, as well as the effect of departures from the assumed geometric and reflectivity characteristics of the actual tracking configuration. Results of processing of real sonar profiles obtained at sea with a man-madeobject of cylindrical geometry are presented, demonstrating the appropriateness of the approach proposed.**

I. INTRODUCTION

This paper proposes a new criterion for autonomous tracking of elongated objects lying on the sea floor with a profiler sonar scanning the vertical plane orthogonal to the robot's direction of motion. Contrary to the majority previously proposed tracking strategies [5,6] – mainly relying in the use of either video cameras, or of muti-beam or side-scan sonar sensors -- the criterion presented here does not rely on the reconstruction, from the sonar measurements, of the local relative robot/object geometry, and considers the use of a simple single-beam mechanically scanning sonar. Obviously, the approach proposed can be transposed to more sophisticated multi-beam sonar systems, with considerable improvemens in the quality and efficiency of tracking. Instead of trying to fit geometric models of the tracked object to distinctive features of the data, and infer from their location the current tracking offset, our tracking approach relies on mantaining a proper balance between the statistical characteristics of the sonar returns sensed from both halves (left and right) of the vertical plane scanned by the sonar. We show that, under mild conditions, driving to zero the tracking error proposed is equivalent to keeping the conic sector scanned by the sonar centred on the object's axis. The computation of the error criterion is entirely based on received sonar data, requiring only an initial step to learn the characteristics of the sea bottom in areas close to the object.

The paper is organised as follows. In the next section we present the platform used in the study and the characteristics of the acoustic sensor on which tracking is based. In section III we present and motivate our tracking criterion, proposing an error measure on the basis of which the reference for a low-level rate controller is generated. Section IV presents simulation results that illustrate the performance and limitations of the approach proposed. Results on real signals acquired at sea are presented in Section V, confirming the appropriateness of our guidance criterion, and its robustness with respect to assumed modeling conditions. Finally, in Section VI we summarize the contributions of the paper.

II. PLATFORM AND SENSOR

A Platform

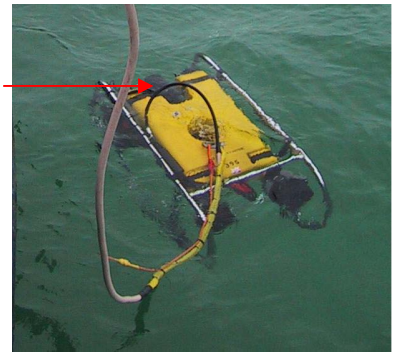

Fig 1: The Phantom being launched at sea.

The underwater platform used in this study is the ROV Phantom,[1] shown in Figure 1. This robot is equipped of three thrusters, two allowing control in the horizontal plane (forward/reverse, turning) and another controlling

[1] Phantom is a Remotely Operated Vehicle (ROV) produced by Deep Ocean Engineering, USA, which has been made available for research in underwater robotics at I3S through a special educational arrangement.

the motion in the vertical plane (up/down motions), and of the following navigation and perception sensors: a magnetic compass, a rate gyro, a pressure (depth) gauge, an altimeter, a profiler sonar mounted on a tilt platform and a video camera. Moreover, each axis is equipped of sensors allowing the measurement of the rotation speed of the corresponding motor axis. The vehicle is linked to a dry-end operational station through an umbilical cable of about 120 meters, which allows remote automatic control of the robot by on-shore PCs.

B Sensor

The sensor used to scan the sea bed is a dual frequency Tritech Seaking profiler Sonar, mounted in a tilt platform in front of the Phantom, see Figure 1. In the configuration used in this study the frequency of the emitted signal is 1.2 MHz, (conical) beam-width is equal to 1.4°, and a maximal range of 7 meters has been set. We assume that the sonar is mounted on the platform such that it scans a plan approximately perpendicular to the sea bottom in a direction approximately orthogonal to the robot's motion. It is further assumed that the angular sector scanned is symmetric, approximately centered in the vertical to the sea bottom.

In Figure 2 we show one complete scan obtained at sea, in the configuration assumed in this paper, and where the circular section of a pipeline lying on the (approximately planar) sea bottom below the robot is clearly discernible. The red vertical line in this Figure indicates the direction corresponding to a zero scanning angle.

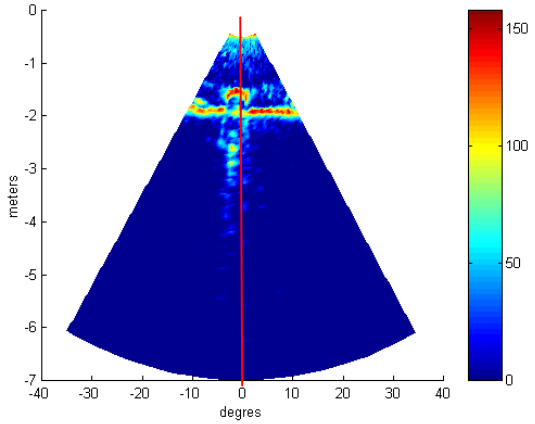

Fig 2. Example of one scan of a pipeline obtained at sea. The color bar in the right indicates the scale of the intensity of the received profiles.

Note that, even if the geometry of the tracked pipeline/seafloor is distincly observable in Figure 2 from the locus of largest intensity of the returned profiles, our algorithm does not rely on this "distance" information. Alternatively, it exploits the distinct reflectivity characteristics of the materials composing the sea-bottom and the tracked object, which lead to distinct shapes of the returned profiles around the distance of maximal intensity, as shown in Figures 3 and 4, where examples of profiles from a pipe (in Fig. 3) and from the sea bottom (Fig. 4) are displayed. In this manner, our guidance criterion is robust with respect to knowledge of the detailed robot motion during scan acquisition, and is also able to handle partially buried objects.

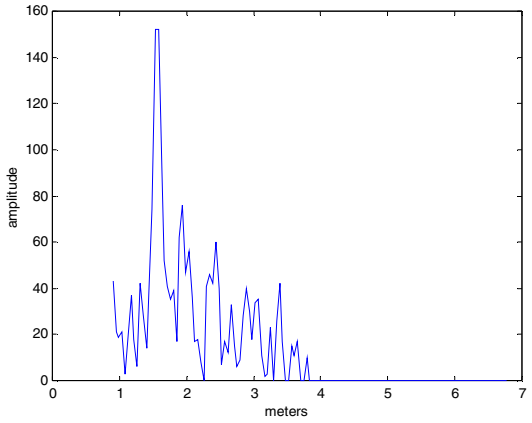

Fig 3: Example of profile received from the pipeline.

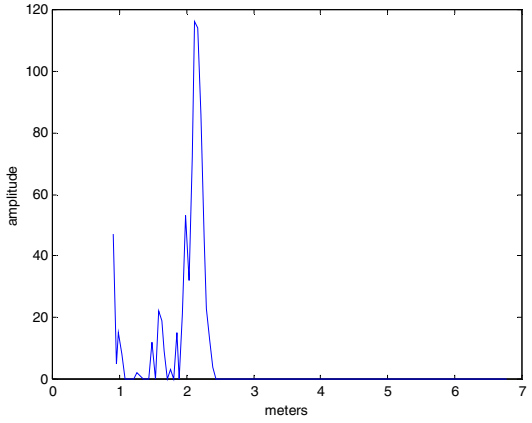

Fig 4: Example of profile received from the seafloor.

III. TRACKING CRITERION

In this section, we present our guidance criterion, which is based on driving to zero an error measure completely defined by the set of profiles acquired during each sonar scan.

We consider the guidance problem only in 2D (in the horizontal plane), asssuming that a separate control loop keeps the platform at a constant altitude from the sea bottom.

As we said before, instead of attempting a local geometric reconstruction of the observed object's shape, which is prone to instabilities in the presence of measurement outliers, and requires reconstruction of the robot motion during scan acquisition, our control signal is a function of the empirical distribution of features of the profiles received inside each complete sonar scan. Moreover, no particular cross-sectional geometry of the tracked object is assumed, the algorithm requiring only that it varies slowly along the object longitudinal axis.

A. Notation

We first introduce some nomenclature and notation. Let X be a discrete random variable (*rv*) with probability space

(Ω,A,P) where $\Omega=\{a_1,a_2,...,a_L\}$ is the (finite discrete) realization space, A is a sigma-field of subsets of Ω and P is a probability measure. We denote by lower-case letters x the realizations of X. Consider a sequence $x^{(n)}=\{x_1,x_2,..,x_n\}\in\Omega^n$ of n independent realizations of X. The empirical estimate of the probability distribution (*pd*) of X is given by:

$$v_{x^{(n)}}(a_j)=\frac{1}{n}\sum_{i=1}^{n}1_{a_j}(x_i),\ j=1,..,L \qquad (2)$$

where $1_{a_j}(x_i)=\begin{cases}1, & x_i=a_j\\ 0, & x_i\neq a_j\end{cases}$

Consider that at instant k we are given the sequence $x_k^{(n)}$ of length n:

$$x_k^{(n)}=(x_1,..,x_n),$$

of n independent realisations of the discrete *rv* X. In the problem addressed in this paper, the sequence $x_k^{(n)}$ corresponds to one complete sonar scan of the angular sector $[-\Theta,\Theta]$ with a step $\frac{2\Theta}{n}$.

As we mentioned previously, we assume the existence of features that enable the discrimination between sonar profiles received from the tracked object and those received from the sea bottom. Moreover, we assume that these features follow *unknown* probability distributions $p_i, i=1,2$, such that the empirical distribution of the n profiles received inside each complete scan will in general be a mixture of these two probablity laws:

$$x_k^{(n)}\propto wp_1+(1-w)p_2 \qquad (3)$$

where the mixture weight $w\in[0,1]$.

We further consider that the unknown distributions $p_i, i=1,2$, vary slowly along the object main axis, in the continuity of the work presented in [3]. We stress again that these features do not necessarily include the measured sonar distances, enabling tracking of objects that do not stand out of the sea floor:

Without loss of generality, we consider that p_1 is the distribution of the profiles received from the *sea bottom*, and p_2 of those received from the *tracked object*.

B. Tracking citerion

Our guidance criterion steers the robot in the horizontal plane such that the *distribution of the profiles received from each half angular sector is at the same "distance" (in distributional sense) from the distribution of profiles received from the sea bottom*. Let $x_{k\pm}^{(n/2)}$ be the data corresponding to the positive ([0, Θ]) and negative ([-Θ, 0]) scanning angles. Since both half scans will in general contain returns from both the seafloor and the tracked object, each of these sequences follows a distribution that is a mixture of p_1 and p_2:

$$x_{k+}^{(n/2)}\propto w_+p_1+(1-w_+)p_2, \qquad (4.a)$$

$$x_{k-}^{(n/2)}\propto w_-p_1+(1-w_-)p_2, \qquad (4.b)$$

for some mixture coefficients $w_{+/-}$ in the unit interval.

Our goal is to drive the robot such that the following equality is maintained:

$$D\left(\nu_+^{n/2}||p_1\right)=D\left(\nu_-^{n/2}||p_1\right) \qquad (5)$$

where $\nu_+^{n/2}$ ($\nu_-^{n/2}$) is the empirical estimate of the probability distribution for the positive (negative) scanning angles, and

$$D(\nu\|p)=\sum_{j=1}^{L}\nu(a_j)\ln\frac{\nu(a_j)}{p(a_j)}$$

is the Kullback-Leibler divergence between probablity laws.

Criterion (5) not requires the segmentation of the individual received profiles into bottom and object classes, but only the computation of the collective empirical distributions of the data received from positive and negative scanning angles.

For instance when tracking a cylindrical pipeline, and if the sonar axis (zero scanning angle) coïncides with the vertical direction, our controller drives the centre of the sonar along the pipe's axis, as the simulation results in Section IV demonstrate.

The error signal that the controller must drive to zero is derived from the Eq. (4):

$$\varepsilon_k\equiv D\left(\nu_+^{n/2}||p_1\right)-D\left(\nu_-^{n/2}||p_1\right) \quad . \qquad (6)$$

Computation of this error signal requires only knowledge of the distribution of the seafloor returns, p_1. An estimate $\hat{p}_1$ of this probability distribution must thus be learned beforehand, for instance by manually driving the robot in neighbooring regions before actual tracking is engaged. The actual error signal is obtained by replacing this estimate for p_1 in equation (6). During tracking this estimate can be adapted to follow smooth local variations.

C. Target Tracking Configurations

We characterise now the possible configurations that lead to a zero (equilibrium) value of ε_k. When this signal is zero, eq. (5) holds, meaning that the two empirical distributions are *equidistant* from the bottom distribution p_1. From equations (4.a) and (4.b), we know that the two empirical distributions fall in the line segment in the probabilistic simplex whose end points are p_1 and p_2. The solution set for $\varepsilon_k=0$ are thus the intersections of this line with the (L-2)-dimensional surface over which the distance to the "centre" distribution p_1 is constant (the "sphere" in Kullback-Leibler "metric"). As we show below, the distance $D(\nu(w)||p_1)$, where $\nu(w)=wp_1+(1-w)p_2$, is a decreasing function of $w\in[0,1]$, and thus that there is a single point of the mixture family at a given distance of one of its end points.

Taking derivatives with respect to the mixture coefficient *w*,

$$\frac{d}{dw}D\left(\nu(w)\|p_1\right)=\frac{d}{dw}\sum_i\left(wp_1(i)+(1-w)p_2(i)\right)\ln\frac{wp_1(i)+(1-w)p_2(i)}{p_{1(i)}}$$

which leads to the follwing expression for *d D(v(w)||p1)/dw:*

$$\sum_i\left(p_1(i)-p_2(i)\right)\ln\frac{wp_1(i)+(1-w)p_2(i)}{p_1(i)}+\left(p_1(i)-p_2(i)\right) \qquad (8)$$

Where it can easily be cjecked that the sum of the second term of the r.h.s. is equal to zero. Using the convexity of the logarithm, we can establish the following upper bound for *d D(v(w)||p1)/dw*:

$$<\sum_i\left(p_1(i)-p_2(i)\right)\left[w\ln p_1(i)+(1-w)\ln p_2(i)-\ln p_1\right],$$

where the strict inequality stems from assumption that the two distrbutions differ at least for one value of *i*. This last expression can be finally rewritten as

$$\sum_i\left(p_1(i)-p_2(i)\right)(1-w)\frac{p_2(i)}{p_1(i)}=-(1-w)\left[D\left(p_1\|p_2\right)+D\left(p_2\|p_1\right)\right]$$

yielding a simpler expression for the upper bound on the derivative *d D(v(w)||p1)/dw* . Since *w* is in the unit interval, both factors in the r.h.s. of the previous expression are positive, demonstrating that the derivative is negative for all values of *w*, and thus the distance *D(v(w)||p1)/* monotonically decreasing along the mixture line, when *w* varies between 0 and 1. This shows that there is a single point where the equality (5) can be achieved, and thus that $\varepsilon_k=0$ implies that the two empirical distributions are the same:

$\varepsilon_k=0 \Leftrightarrow \nu_-^{n/2}=\nu_+^{n/2}$.

Equality of the distributions corresponding to the two semi-planes (positive and negative scanning angles) means that both half scans contain the same percentage of bottom and object returns, *i.e.*, $w_-=w_+$. Since we assumed that the complete scanned angular sector is symmetrical, this in turn implies that the sonar vertical axis intersects the object at its cross-sectional symmetry axis, see Fig. 5.b).

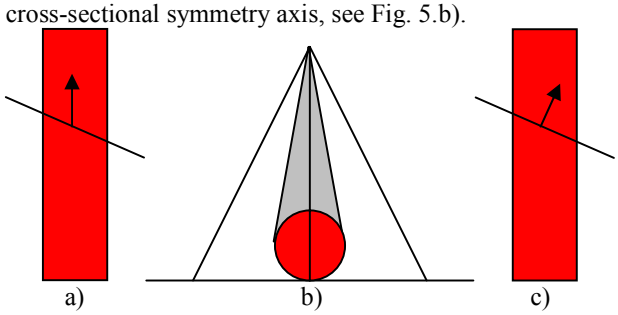

Fig 5. a) Stationary tracking situatio with a skewed sonar plane (top, view, the arrow indicates the direction of motion of the platform); b) stationary perfectly aligned situation (front view); c) transient situation: the skewed scanned plan is due to a wrong robot direction.

Note that $\varepsilon_k=0$ can be attained even if the scanned vertical plane is not orthogonal to the object's axis, see Figures 5.a) and c). If this situation to correspond to a stationary solution of the closed loop system presented below, see eq. (7), we must still impose that the derivative of ε_k is zero. This will be the case only if the sonar presents a skew angle with respect to the direction of motion of the robot as in Fig. 5.a) (the proposed controller being robust with respect to this type of misalignements). On the contrary, if the departure from transversality corresponds to a robot trajectory that is not parallel to the object's axis, as in Fig. 5.c), the error derivative will be different from zero, and the closed loop system will converge to an aligned situation.

Note that the above discussion is independent of considerations concerning an eventual lateral rotation of the sonar (a fixed roll angle) on the robot's frame, as shown in Fig. 6.: the sonar coordinate axis will still be centred in the object. Our approach is thus also robust with respect to this kind of offsets, whose net effect is to induce a non-zero offset between the trajectory of the sensor and the object's axis: the trajectory will still be parallel to the object, but at a given constant distance from its centre.

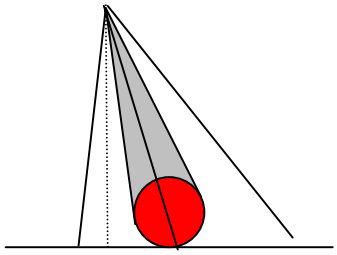

Fig 6. Effect of a non-zero roll offset of the sonar frame (front view). The dotted line is the projection of the origin of the sonar frame in the sea floor, indicating a lateral offset of the robot trajectory with respect to the object's axis.

D. Observability of the distance to the object's axis

The controller presented in [4], and on which rely to drive to zero the error signal ε_k was developped for an error measure that is proportional to the orthogonal distance between the platform and the tracked line. We assess in this subsection the validity of this linear assumption for the error signal given by (6).

Let *r* denote the maximal percentage of the complete sonar scan that is received from the tracked object (for instance, for the situation in Fig. 6, $r<0.5$). It is related to the mixture coefficients of the distributions in each half scan by

$r=(w_+ + w_-)/2 \Leftrightarrow w_-=2r-w_+$.

Since the mixture coefficients must belong to the unit interval, we see that $w_+ \in [\max(2r-1,0), \min(2r,1)]$. The nixture coefficient is related to the lateral offset d of the object and to the tracking altitude *h* by the following equation

$\mathrm{tg}(\Theta w_+) = d/h + \mathrm{tg}(\Theta r)$.

Using the chain rule of derivation, we can write

$d(\varepsilon_k)/d d = d(\varepsilon_k)/dw_+ \; . \; d(w_+)/d d$.

Using the previous expression,

$d(w_+)/d d = \cos^2(\Theta w_+)/(\Theta h)$.

We derived in the previous subsection the expression of the derivative of the Kullback-Leibler distance along the

mixture family, eq. (8). In Fig. 7 we plot the evolution of the error signal ε_k as a function of the mixture coefficient w_+ in the linearity interval corresponding to several distinct values of r. For the following figures, we considered $h=7$ metres, and $\Theta=\pi/8$. The two distributions p_1 and p_2 were randomly chosen in the probabilistic simplex, and the results presented are representative of the behaviour observed for other choices.

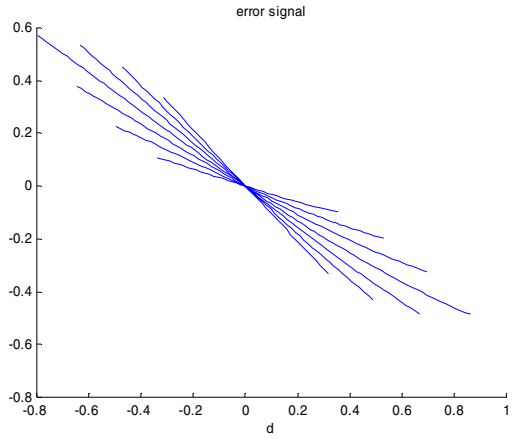

Fig 7. Variation of the eror signal as a function of the horizontal offset between sensor and object's axes.

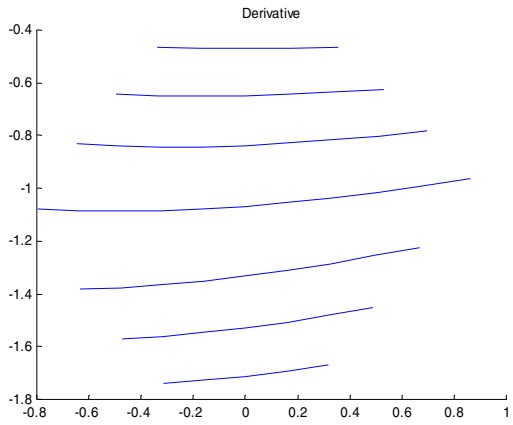

Fig 8. 1st derivative of the error signal.

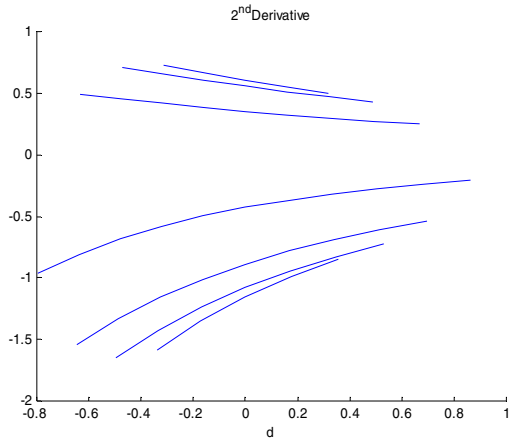

Fig 9. 2nd derivative of the error signal.

Outside this region of "linearity" (where the interaction of the finite opening of the scanned angular section is not felt), saturation effects imply a decrease of the asolute value of the error signal. As we can see the error signal presents, over this limited region a variation approximately proportional to the distance between the sonar axis and the object axis of symmetry. Figures 8 and 9 display the 1st and 2nd derivatives of the error signal with respect to the distance d. As we can see, the 1st derivatives are approximately constant for al values of r considered, the 2nd derivatives being small (we stress that in a Taylor development of the error signal, these derivatives are multiplied by the powers of the mixture coefficients, which is smaller than 1).

E. Controller structure

As it is fully motivated in [4], the natural control parameter to track a horizontal line is the curvature κ of the robot trajectory at each point (the derivative of the platform's yaw angle with respect to arc length). The sonar-derived error signal is thus used to drive a proportional-derivative controller whose output sets the reference value for a low-level rate controller:

$$\kappa_k = K_p \varepsilon_k + K_d \left(\varepsilon_k - \varepsilon_{k-1} \right), \qquad (6)$$

This controller is completely driven by the perception-derived error signal ε_k, and thus independent of the assumed dynamic and kinematic platform models (which obviously must be properly taken into account when designing the low-level rate controller), increasing its robustness with respect to modeling errors. A word must be said with respect to determination of the controller gains. In [4], it is shown how the controller gains (proportional and derivative) must be set according to the local variation of the sensed signal with respect to the orthogonal distance between the platform and the tracked line. In that case, we were adressing tracking of a level line of a scalar field using a point sensor of the value of the field. In the case considered here, correct setting of the controller gains will require (besides knowledge of the control rate and the vehicle surge speed), an indication of the derivative of the Kullback-Leibler distances with respect to the robot (sonar) offset with respect to the centre of symmetry of the tracked object. This derivative can be seen to depend on the particular distributions p_1 and p_2, or can be estimated locally. This problem is a topic of current study, and will be adressed in future publications.

IV. SIMULATIONS

In this section we present simulation results of the tracker described in the previous sections, considering complete system simulation of the motion in the horizontal plane (including thruster dynamics and low level control loops). The robot was driven at a nominal surge speed of 0.15 m/s, control rate is 10 Hz, and sonar rate (rate of classified sonar profiles) is 20 Hz (operating height is 2

meters). Sonar scanning parameters are $\Delta\phi = -0.5$ and $\theta = 5°$. Controller gains are $K_p = 0.64, K_d = 4$.

The first example, see Fig. 10, considers tracking of a linear pipeline of diameter 0.2m. We consider a perfectly aligned system: the scanned plan is vertical, orthogonal to the robot's direction of motion, and that the sea plane is perfectly flat and horizontal.

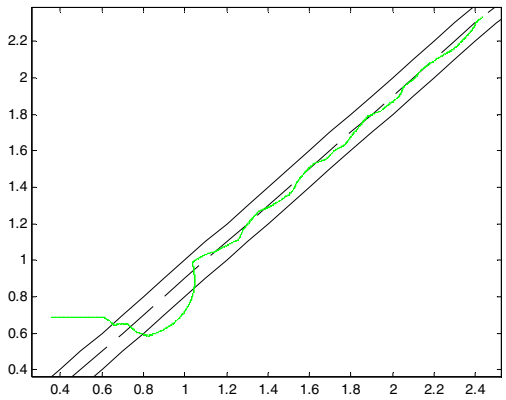

Fig 10: Case 1. Tracking of a straight pipeline.

To appreciate the behaviour of the proposed tracker, we plot in Fig. 11 the North component of the error between the robot's trajectory and the axis of the pipeline:

$$e_{traj} = \sqrt{(y_d - y_r)^2} \qquad (7)$$

where (y_d) represents the desired coordinate and (y_r) the real coordinate. As we can see, this error decreases to zero, reflecting the damped oscillations of the trajectory around the desired linear path, as it has been theoretically predicted in [4].

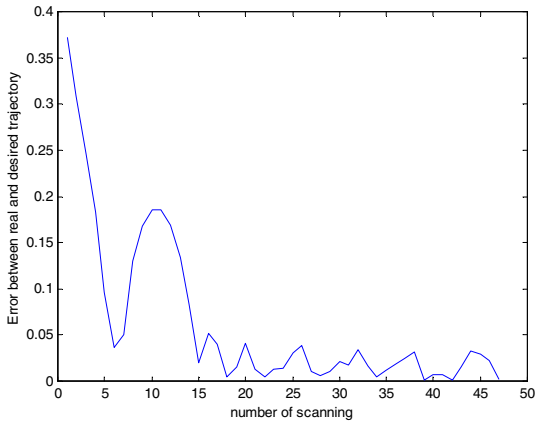

Fig 11: Error of tracking.

The second example, see Fig. 12, considers tracking of a pipeline containing a right angle turn. The corresponding evolution of the tracking error is plotted in Fig. 13. We can see that the controller is able to maintain tracking, being able to cope with the saturation of the error signal resulting from sudden change in the pipe's orientation, the error signal tending to zero following again a damped sinusoidal behavior.

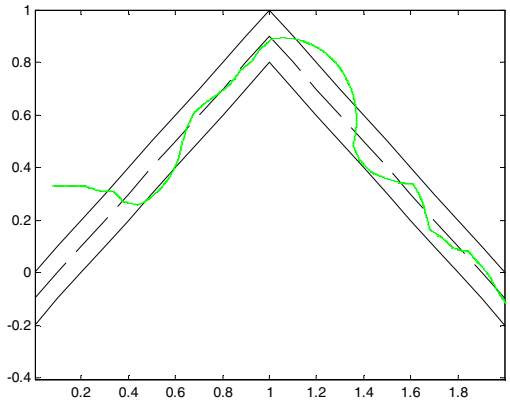

Fig 12: Tracking at a right angle turn.

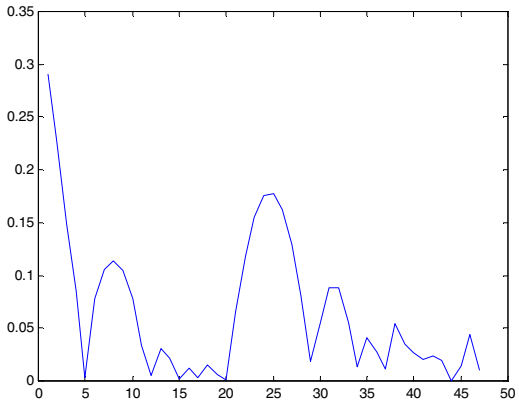

Fig 13: Tracking error.

The simulation illustrated in Figures 14 and 15 illustrates the robustness of the method to variations of the seafloor reflectivity characteristics during tracking. To test the behaviour with respect to bottom assymetries (our criterion is implicitely based on a symmetry assumption concerning the two sides of the tracked object) this variation has been imposed only on one side of the pipeline.

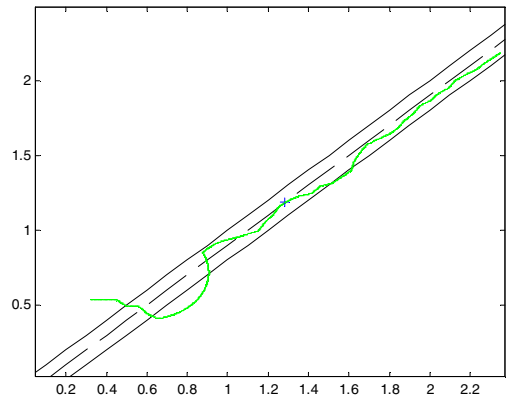

Fig 14. Tracking under seafloor variation along track (the variation begin after the blue cross).

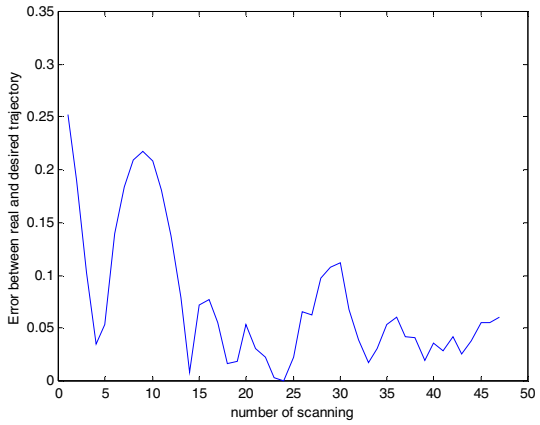

Fig 15: Tracking error. Seafloor variation occurs after scan 25.

We can see that after an initial trasient period (which is mainly due to the response of the proportional-derivative controller to the sudden model change), the robot continues to track the pipe, but with an offset with respect to its center.

V. RESULTS ON REAL DATA

In this section we present results of processing real data aquired during contolled experiments at sea. For these experiments pipeline sections have been layed in the sea bottom in a coastal region of the South of France, near Toulon. The Phantom has been manually driven along the pipe, using the on-line video returns. We note that the turbidity of the water offered a reduced visibility of the pipe during these experiments, explaining the large oscillations observed in the acquired data.

To analyze the performance of the tracking criterion on this data, we compare the sign of ε_k given by equation (6) with the position (left/right) of the center of the pipeline with respect to the sonar axis, manually detected for each scan (see Fig. 2). According to our conventions, $\varepsilon_k>0$ if the pipeline is on the right of the sonar axis and negative when it is on the left. For instance, for the scan in Fig. 2, the error signal should be negative since the pipeline is slightly on the left of the sonar axis (red vertical line). A total of 100 scans have been analyzed, yielding 84 good sign indications of the method. In Fig. 14 we plot the value of ε_k versus the angular position θ_k^{pipe} of the centre of the pipeline with respect to the sonar zero scanning direction, manually extracted for each scan. As this figure shows, the situations where the lateral (left/right) indication of our criterion is wrong (indicated by '+' signs in the plot) appear, except in one case, always for pipe directions close to 0°, and are due to the variability linked to the determination of an histogram from a small volume of data. Note that we cannot compare directly Fig. 16 to the Fig 7, because the robot's altitude above sea bottom has not been kept constant during this experiment.

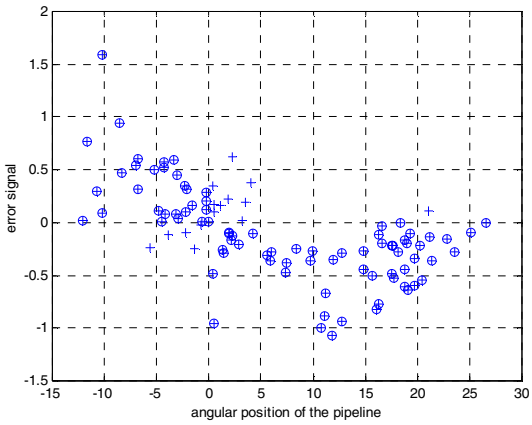

Fig 16: Error signal ε_k versus angular position of the pipeline. Crosses indicate the samples with wrong left/right indication.

Finally, in Figures 17 a) and b) we show examples of two distinct scans, along with the indication of the corresponding values of ε_k. We can see that in b), where there is a larger offset between the sonar axis and the pipeline, the value of the error signal is larger than in a). In both cases the left/right indication is correct.

VI. CONCLUSIONS

We presented a criterion that enables tracking of an elongated object lying on the sea floor by a mobile robot equipped of a scanning profiler sonar. The proposed tracking criterion does not require detailed reconstruction of the geometry of the tracked object, nor of the robot's trajecotry during tracking. In particular, it can handle partially buried objects. The error signal is directly derived from enforcing a symmetry condition between the empirical distributions of the two each half-scanned angular sections. The performance of the tracking error proposed has been studied in simulation, under violation of several of the nominal assumptions that underly the approach. Preliminary results on real data acquired at sea indicate that the algorithm can cope with the uncontrolled conditions of true field operations.

REFERENCES

[1]. G. Tascini, P. Zingaretti, G. Conte, S.M. Zanoli. Perception of an underwater structure for inspection and guidance purpose.1st EUROROBOT, Kaiserslautern, Germany, 1996.

[2]. Y. Petillot, S. Reed, J. Bell. Real Time UAV Pipeline Detection and Tracking using Sidescan Sonar and Multi-Beam Echo Sounder. MTS/IEEE Oceans Conf. Mississippi, US, 2002.

[3]. C. Barat, M. J., Rendas. Tracking Benthic Boundaries Using a Profiler Sonar: a mixture model approach, Proc. Oceans 2003, San Diego, USA, 2003.

[4]. Maria-João Rendas, Isabel Lourtie, Georges Pichot, Adaptive Sampling for sand bank mapping using an autonomous underwater vehicle equipped of an altimeter, ISESS 2003, Vienna, Austria, May 2003.

[5] PG. Tascini, P. Zingaretti, G. Conte, S.M. Zanoli, Perception of an underwater structure for inspection and guidance purpose, 1st Euromicro Worskshop on Advanced Mobile Robots (Eurobot), 1996.

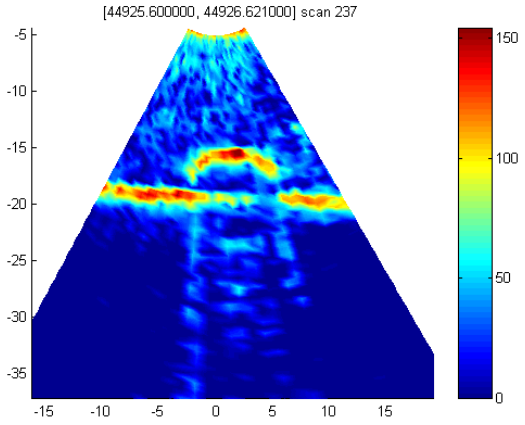

a)

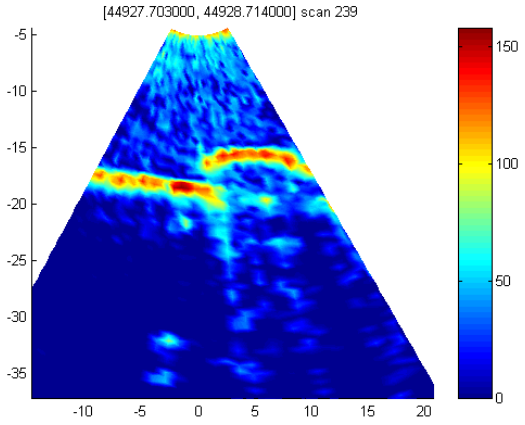

b)

Fig 17: Two distinct real sonar scans. a) ε_k=0.27 ; b) ε_k=0.82 .